In-situ versus laboratory characterization of historical site in marine environment using X-ray fluorescence and Raman spectroscopy

F.F. Mendonça Filho, H. Morillas, Hannelore Derluyn, M. Maguregui, David Grégoire

▶ **To cite this version:**

F.F. Mendonça Filho, H. Morillas, Hannelore Derluyn, M. Maguregui, David Grégoire. In-situ versus laboratory characterization of historical site in marine environment using X-ray fluorescence and Raman spectroscopy. Microchemical Journal, 2019, 147, pp.905-913. 10.1016/j.microc.2019.02.014 . hal-02047142

HAL Id: hal-02047142
https://hal.science/hal-02047142

Submitted on 6 Oct 2022

HAL is a multi-disciplinary open access archive for the deposit and dissemination of scientific research documents, whether they are published or not. The documents may come from teaching and research institutions in France or abroad, or from public or private research centers.

L'archive ouverte pluridisciplinaire **HAL**, est destinée au dépôt et à la diffusion de documents scientifiques de niveau recherche, publiés ou non, émanant des établissements d'enseignement et de recherche français ou étrangers, des laboratoires publics ou privés.

In-situ versus laboratory characterization of historical site in marine environment using X-ray fluorescence and Raman spectroscopy

F. F. Mendonça Filho[a,1], H. Morillas[b,*], H. Derluyn[a,**], M. Maguregui[c], D. Grégoire[a,d]

[a]*CNRS / TOTAL/ Univ Pau & Pays Adour / E2S UPPA, Laboratoire des Fluides Complexes et Leurs Reservoirs - IPRA, UMR5150, 64600, Anglet, France*
[b]*Department of Analytical Chemistry, Faculty of Science and Technology, University of the Basque Country UPV/EHU, P.O. Box 644, 48080, Bilbao, Spain*
[c]*Department of Analytical Chemistry, Faculty of Pharmacy, University of the Basque Country UPV/EHU, P.O. Box 450, 01080 Vitoria-Gasteiz (Alava, Spain)*
[d]*Institut Universitaire de France, France*

Abstract

–

Accepted manuscript in *Microchemical Journal*.
DOI: 10.1016/j.microc.2019.02.014.
The final publication is available at:
https://dx.doi.org/10.1016/j.microc.2019.02.014

–

Raman spectroscopy and X-ray fluorescence spectrometry are powerful analytical techniques that allow for molecular and elemental analysis, respectively. Recent developments allowed for the miniaturization of equipment to an extent that in-situ experiments become available. There are many advantages in using portable instruments, but this requires sacrifices regarding

*Corresponding author UPV
**Corresponding author UPPA
Email addresses: f.filho@tudelft.nl (F. F. Mendonça Filho), hector.morillas@ehu.eus (H. Morillas), hannelore.derluyn@univ-pau.fr (H. Derluyn), maite.maguregui@ehu.eus (M. Maguregui), david.gregoire@univ-pau.fr (D. Grégoire)
[1]Current address: Microlab, Faculty of Civil Engineering and Geosciences, Delft University of Technology, Stevinweg 1, 2628CN, Delft, The Netherlands

the acquisition of the spectra and the quality of the analysis. How much information is lost with this exchange is not clear, neither how important this is for the use of these techniques as forensic tools. In this work, the damage of a façade of Villa Belza, a historic building in Biarritz, France, was evaluated using both portable and benchtop versions of X-ray fluorescence (XRF) and Raman spectroscopy and the approaches were compared. As the comparison of instruments designed for different conditions is not straightforward, the authors use a number of settings to discuss what would be a realistic juxtaposition of results and how this affects the diagnosis of the structure. Furthermore, some hand-held XRF spectrometers are not connected to appropriate software to proceed with the data treatment and the processing of such signals can be tedious or too time consuming. Thus this work also proposes an algorithm for the automatic identification and comparison of elements in the XRF spectra acquired on site. After discussing the trade-off involved with each technique and the respective effect in the limit of detection, the authors conclude that the extra information from benchtop instruments was negligible for this case study.

Keywords: in-situ analysis, X-ray fluorescence, Raman spectroscopy, stone weathering

---

1. Introduction

Marine salts are easily carried by wind, which represents cumulative deposition in near sea structures. Given common environmental changes, namely, the variation of temperature and relative humidity, these salts go through dissolution and precipitation cycles that can cause both mechanical and chemical damage [1, 2]. The interaction of building materials with those salts is rather complex, with multiple effects taking place simultaneously [3, 4].

One of the most common forms of deterioration is the cracking and subsequent loss of material by the crystallisation of the salts in pores (subflorescence). If the crystallization occurs on the surface, it is called efflorescence and the only damage is aesthetic. However, underneath the surface, crystallization pressure can exceed the capacity of the material in a sufficiently large volume to create a fracture, which is driven by the generation of supersaturation in the solution [5]. Common mechanisms that cause such levels of supersaturation in nature are, the drying of a material imbibed with a saline solution, inducing salt precipitation at the location of the drying front, or

the change between phases of a salt in which the solution is in equilibrium for one phase and supersaturated with respect to another (as is the case for sodium sulphate conversion from mirabilite to thernadite) [6].

Additionally, the presence of certain compounds can create favourable conditions for the extraction of calcium from calcite ($CaCO_3$) and Portlandite ($Ca(OH)_2$), two of the major components of stone and mortar. This is often seen in building materials contaminated with sodium sulphate [7, 8] or nitrates [9, 10]. The dissolution of such phases combined with humidity cycles causes leaching, which can significantly increase the porosity of the matrix while reducing its strength [11, 12] in addition to the aesthetic damage.

Thus, the visual identification of salts in coastal structures can signalise different processes taking place. In order to perform preventive or corrective measures, it is first necessary to identify the dominant form of damage, which usually requires knowledge of present compounds and comparison with undamaged material.

Raman spectroscopy and X-ray fluorescence (XRF) are very popular techniques with vast applications in archeology [13, 14], art conservation [15, 16], and, more recently, built heritage preservation [17, 18]. The use of Raman analysis provides molecular characterization, which can aid in the inference of reactions taking place in the studied medium. In the context of construction materials, this technique can identify both main components and trace elements of building stones and cementitious materials in addition to common nitrates and sulphates and some of their degradation products [9, 19]. On the other hand, X-ray fluorescence provides elemental composition. This type of information can help to distinguish between similar materials or even trace back their origins [20] or type [21]. Also, the ingress of aggressive agents can be detected and quantified [22].

Current developments allowed for the miniaturization of such instruments to a degree of field use being possible. In the construction industry, in-situ analysis avoids a number of problems associated with coring [23], such as: damaging of the sample's microstructure by the mechanics of extraction; the exposure of inner sections to the atmosphere, allowing reactions with common gasses; the need for re-sampling posterior to analysis; and others. In the cultural heritage field, the use of this type of analysis presents the possibility of a completely non-destructive characterization, avoiding the loss of historical patrimony [24, 25]. Thus, there is a big interest in the passage from laboratory techniques to in-situ analysis. However, it is not clear how much

information is lost by using only portable devices, and more importantly, how significant that loss is for the overall evaluation.

The focus of the present work is in the comparison between the data extraction, processing and analysis of hand-held instruments against their benchtop alternatives. Specifically, the use of X-ray fluorescence and Raman spectroscopy with the goal of characterizing the state of a historical construction. Attention is given towards the methodology chosen to interpret and compare the data and how this affects elemental sensitivity and the analysis of the results.

Furthermore, commercial devices not previously devoted to research often lack an accompanying software to handle large amounts of data in manageable time, this is the case for the hand-held XRF spectrometer used in this work. Thus, a MATLAB® script was created to read the spectra as given by the instrument, assign an element to each peak and generate a user friendly data output while reducing the processing time from many hours to tens of seconds. The accuracy and limit of detection of such algorithm is compared to the manual procedure and both are judged based on what was found in the analysis performed in the laboratory.

2. Materials and methods

2.1. Sampling and in-situ campaign

The object of study was a five stories building called Villa Belza, built from 1880 until 1895. The construction is situated in the coast of Biarritz, France, with direct exposition to sea spray (Figure 1, top). In 2017 the owners decided to perform a renovation due to severe deterioration of the façade. Upon inspection, a number of points presented precipitation of salts and loss of material at the surface, thus, many samples were extracted prior to the renovation works, in order to determine the causes of deterioration. This paper presents the analysis of the material on the ground entrance from the south-east direction (Figure 1, bottom).

As it can be seen, the location had different materials composing the entrance, nine points were chosen to represent all structural components there. The location of all points is denoted in red in Figure 1, bottom. For simplicity, the stone samples were named S1 to S4 and the mortar samples M1 to M5. Samples S1 and S2 were composed of limestone, S3 was Bidache stone, S4 was made of the natural stone at this location, M1 to M4 were render-

Figure 1: Top, left: Location of Villa Belza in France. Top, right: Satellite photo of structure. Both top images are provided by Google Maps, the red arrow represents the direction and position of the image on the bottom right. Bottom, left: Southeast view of Villa Belza as of 2014 [26]. Bottom, right: Position of each sample regarding the location of in-situ analysis and core extraction.

ing mortars of a recent restoration, and M5 was a mortar from a previous restoration with unknown age.

In order to obtain representative results on each sampling area and each material type, at least three were acquired in-situ using the portable instruments. In this way, more than three Raman spectra and six XRF analyses were acquired per location and thereafter cores were extracted. XRF had six tests because two settings of the X-ray tube were used to detect not only

heavy elements, but also the light ones, as described elsewhere [21]. After in-situ studies, the cores were brought to the laboratory, where Raman and XRF spectra were collected with benchtop instruments, taking care to analyse the exposed face that was previously analysed in-situ.

2.2. Instrumentation

2.2.1. Hand-held instrumentation

The mineralogical composition was determined in-situ through Raman analysis carried out with a portable innoRam spectrometer (B&W Tek Inc., Newark, USA), equipped with a 785 nm excitation laser. The laser power is approximately 300 mW at the source and about 200 mW at the surface of the analyzed sample. The instrument implements a controller of the laser power fixable from 100% to 1% of the laser. The spectral range was acquired between 65 and 3000 cm^{-1} with a resolution of 4 cm^{-1} at 912 nm. The instrument implements a TE cooled (20 ^{o}C) back-thinned, 2D binning CCD detector. Raman spectra were recorded using the BWSpec ^{TM} 3.26 software version (B&W Tek Inc), after a daily calibration with a silicon chip using the 520.5 cm^{-1} Raman line.

The in-situ elemental analysis was carried out using an XMET5100 (Oxford Instruments, UK) hand-held energy dispersive X-Ray fluorescence spectrometer (HH-ED-XRF). The instrument is equipped with a Rh tube working at a maximum voltage of 45 kV. The spot size of the emitted X-Ray beam is 9 mm. The analyzer includes a Peltier-cooled silicon drift detector (SDD) of high resolution that is able to provide an energetic resolution of 150 eV (calculated for the Mn Kα line). The analyzer contains a PDA to control the spectrometer and also to save the spectra and semi-quantitative information. To determine the presence of the heaviest elements (Z > Ti) the voltage and current of the X-Ray tube was set at 40 kV and 15 μA respectively and the spectra were acquired during 100 seconds (real time) in order to improve the signal-to-noise ratio of trace elements. Additionally, to remove the "pinches" Bremsstrahlung and improve the detection of heavier minor and trace elements, a 500 μm Al filter was used. In order to improve the detection of the lighter elements (Z < Ti), additional measurements were performed without the Al filter and at lower voltage (13 kV) and higher current (45 μA) during 70 seconds, real time. To determine possible contributions from the set-up of the instrument (e.g. detector) and possible contaminations of the XRF analyzer window, 20 repetitive spectra of an instrumental blank (a PTFE block) were acquired before each measurement batch. The used PTFE block was

cleaned before its use in a 20% nitric acid bath during 24h. Before its use, it was rinsed in Milli-Q water and dried. Before each measurement batch also the spectrometer energy calibration was checked using the option available in the instrument control software and the metallic surface provided by Oxford Instruments. For the repetitive measurements, the same spectral conditions (voltage, current, filter and test time) as those used for the analysis of the areas under study were considered.

2.2.2. Benchtop instrumentation

For the laboratory micro-Raman analyses, an inVia Renishaw confocal Raman microspectrometer (Renishaw, Gloucestershire, UK) coupled to a DMLM Leica microscope with 5x, 20x and 50x long working distance lens was used. For the analysis of all the building materials from Villa Belza, a 785 nm (nominal laser power 350 mW) excitation laser was used. The laser was set at low power (not more than 1 mW at the sample) in order to avoid thermal decomposition. The spectrometer was calibrated daily by using the 520.5 cm^{-1} Raman band of a silicon chip. Data acquisition was carried out using the Wire 4.2 software package (Renishaw). Spectra were acquired between 105 and 1350 cm^{-1} spectral region, which corresponds to the fingerprint area of the compounds of interest, during 1-10 s and several scans (between 1 and 20) were accumulated for each spectrum in order to improve the signal-to-noise ratio.

The study of the elemental composition in the laboratory was done with an M4 TORNADO Energy Dispersive X-ray fluorescence spectrometer (Bruker Nano GmbH, Berlin, Germany). This instrument is equipped with a micro-focus side window Rh X-ray tube powered by a low-power HV generator and cooled by air. It can work using polycapillar lenses, which allow performing both single point measurements down to 25 μm of lateral/spatial resolution, and Hyper Maps to determine the distribution of each element detected in the collected fragments. Additionally, a second X-ray tube is present using a mechanical collimator, which possesses a spatial resolution of 1 mm, but can avoid secondary effects (e.g. diffraction peaks) created by the polycapillar lenses. The use of a bigger lateral resolution through a mechanical collimation also reduces the X-ray flux on the sample, affecting the limit of detection of the light elements (e. g. Na and Mg). For the focusing of the area under study, two video-microscopes were used, a low magnification one (1 cm^2 area) for the exploration of the sample and a higher magnification one (1 mm^2 area) for the final focusing. The spectral acquisitions in this work were

performed at the maximum allowed voltage (50 kV) and current (600 μA, 700 μA) for each respective tube. A XFlash silicon drift detector with 30 mm^2 sensitive area and energy resolution of 145 eV for Mn-Kα was used for fluorescence radiation detection. In order to improve the detection in a similar manner than with the hand-held device, measures were performed with and without an Aluminium filter of 630 μm. Moreover, measurements were acquired under vacuum (20 mbar), which was achieved with a diaphragm pump MV 10 N VARIO-B. The live time used for each punctual measurement was 300 seconds.

Before each measuring batch, a routine calibration and quality management procedure was applied in order to ensure an acceptable quality of the obtained spectral information. This procedure encompasses the spectrometer energy calibration, and the verification of possible contaminations in the detector and lens alignment. When the polycapillar lens was used, the X-ray spot alignment was also verified. In the case of the 1 mm mechanical collimator it is not necessary to verify it, since the collimation is achieved using a mechanical piece which does not include any lens that can be unaligned prohibiting a deviation in the X-ray spot guided to the sample. The spectrometer energy calibration was done selecting the corresponding maximum pulses according to the used detector, measuring a Zr disc provided by Bruker Nano GmbH and selecting its Kα line for the final energy calibration. The obtained Zr spectrum was included in the calibration control chart in order to control possible decreases in the counts registered for this element and thus, to monitor the live of the X-ray tube. For the X-ray spot alignment verification, a specific surface provided also by Bruker Nano GmbH which allows to observe the X-ray beam was used. If a certain deviation in the alignment is detected, the software implemented allows for its correction. Finally, for the verification of possible contaminations in the detector and lens alignment, the methacrylate inside the instrument chamber where the samples are usually placed was used. A specific measurement at 50kV, 200 mA during 60 seconds under vacuum (20 mbar) was programmed using the set-up of the instrument which includes the polycapillar lens. The measurement was done in a specific XYZ coordinate of the table, to compare the obtained result with previous measurements done in the same position and registered in a control chart. The obtained measurement should be inside the interval of the control chart with an intensity delta (parameter of the software controlling the instrument) lower than 5%.

2.3. Data analysis

The interpretation of the unknown Raman spectra was carried out by comparison with the Raman spectra of pure standard compounds collected in the e-VISNICH dispersive Raman database [27]. Additionally, free Raman databases (e.g. UCL [28] and RRUFF [29]) were also considered for the assignation of Raman bands. The M4 TORNADO software (Bruker Nano GmbH, Berlin, Germany) allowed the acquisition of semi-quantitative element calculation after a previous elemental assignation and deconvolution on the XRF spectra acquired in the laboratory.

Regarding the XRF spectra collected in-situ, the instrument does not possess an interpretation software. The freeware EzData^{TM} can be used to accomplish the task, but it requires manual selection of each peak in each spectra and posterior assignation of elements, which can be very time consuming. For this reason, a MATLAB® script was developed for automation of the process [30]. In the code, the elemental identification is based on the energies published by Barden [31], considering only K and L lines. The algorithm looks for any element with an emission line within a maximum distance d from the center of the peak in question and produces a list. However, using simple peak position as a mean to assign elements has proven ineffective since peaks can shift slightly and conflicts between elements with similar energies in different lines are frequent. Thus, an additional selection criteria was necessary. Wang et al [32] gave a recent estimation of Earth's elemental abundance, which can be used as a probability parameter for overlapping X-ray emission energies. Such parameter creates a bias towards common elements, but in the context of construction and/or natural materials, it is rather useful. To compare all the emission lines collected for a given peak, the smallest value of S is searched according to equation 1.

$$S = \frac{\mathrm{abs}(X_e - X_p) + a}{b + \frac{\log(A_e/A_{Am})}{\log(A_{Fe}/A_{Am})} * (c - b)} \tag{1}$$

X_e is the position of the emission line of element e in keV, X_p is the position of the peak p in keV, a is an empirical parameter for calibration, A_e is the mass abundance of element e in ppm (mg/kg) and A_{Am} and A_{Fe} are the abundance of americium and iron, respectively. b and c are rescaling parameters.

Given the non-linear nature of X-ray fluorescence, a baseline correction is necessary in each spectrum previous to quantification [33]. This is done

using the routine developed by Ning et al [34] for complex spectra. After that, Gaussian curves are fitted under each peak to perform the deconvolution of close emissions and any quantification desired (e. g. net counts, area under the curve, full width at half maximum).

For the parallel analysis of such signals with the laboratory ones, additional considerations were made. When using competing instruments, identical parameters are often set to ensure a fair comparison of their detection capacity. Yet, hand-held devices constrain the analysis in terms of time and geometrical precision simply by requiring human operation, with the additional obstacle of air between the sample and the detector, a weaker signal is normally obtained. An argument could be made that for true comparison, the desktop device should be set to the same acquisition time, using identical current and accelerating voltage with a similar tube and spot size. Notwithstanding, the authors believe this could be interesting from the industrial point of view, but would not fit in the aim of this research, because once a sample is taken to the laboratory extra steps are taken to assure the most accurate detection possible. Therefore, when comparing field analysis with laboratory tests, it is more logical to use the standard procedure for both.

As a compromise, two laboratory analysis were performed. The first one mimics the type of collimator and filters used by the in-situ analysis, which means that a mechanical collimator with spot size of 1 mm was used for measurements without filter and with an aluminium filter of 600 μm. The second one uses a polycapillar collimator and no filter. However, both were performed in vacuum with a longer exposure time for each point than the in-situ counterpart. It was chosen to use no filter for the second analysis after a brief comparison of elemental detection, as can be seen in Figure 2.

3. Results and discussion

3.1. Raman spectroscopy

The in-situ Raman analysis of the studied areas from Villa Belza revealed mostly calcite peaks, which is in agreement with the laboratory analysis of samples S3 and M2 to M5. The presence of other phases was detected in the remaining samples during the laboratory analysis as demonstrated by Figure 3.

In sample S1 there is a weak peak at 1008 cm^{-1}, which can be attributed to gypsum ($CaSO_4 \cdot 2H_2O$). This was present in many points of this sample and points to a well distributed phase. The other peaks at 156, 282, 712, 1086

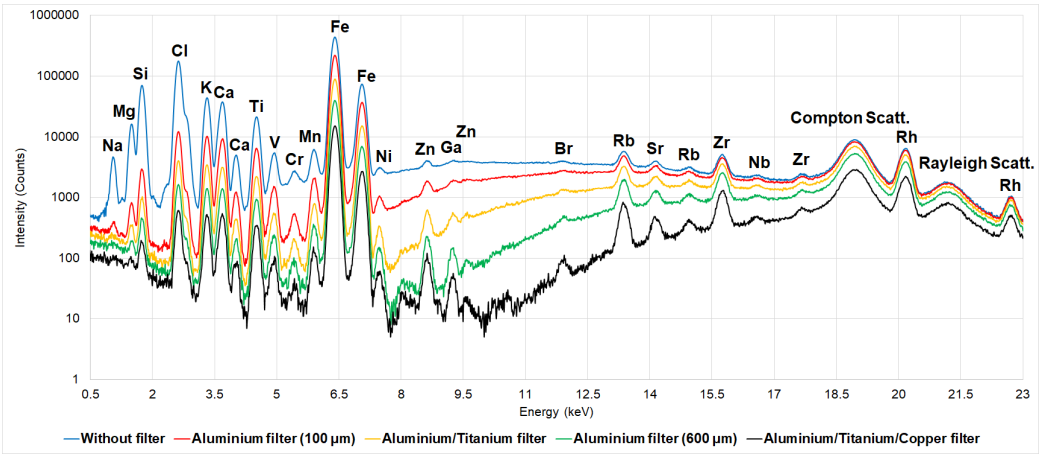

Figure 2: Comparison of detection power using different filters implemented in the M4 TORNADO ED-XRF spectrometer applied to sample S3 as example of signal improvement.

cm^{-1}, are commonly attributed to calcite, and similar to the field analysis, were present in all analysed surfaces. Sample S2 also presents the usual peaks of calcite in all surfaces, but a secondary greenish phase was observed with peaks at 1063, 1128, 1296 cm^{-1}. Huang et al [35] states that all saturated fatty acids have similar strong peaks in the same shifts, thus, it is likely that this is the contribution of animal contamination. In sample M1, besides calcite, quartz (α–SiO_2, Raman bands at 207, 463 cm^{-1}) and gypsum (Raman bands at 413, 493, 617, 670, 1008, 1135 cm^{-1}) were found. The presence of both is common in mortars. Sample S4 had few points that showed haematite (Fe_2O_3, with its Raman peaks at 219, 242, 286, 403, 488, 606 cm^{-1}), but calcite was still the dominant phase.

The predominant presence of calcite in the mortars could be used as an argument for carbonation of the material, but since only the surface was analysed, this is an expected result. The first millimetre of even new mortars would carbonate in a relatively young age, hence the decades old mortars could even be completely carbonated. Although carbonation is a major concern for reinforced structures, unreinforced mortars composed of Portland cement tend to become more compact, in which case this can be seen as an advantage against external agents, such as decreasing the rate of leaching [36] or slowing down the ingress of chlorides [37, 38, 39].

Finally, an useful observation from the Raman analysis of the samples

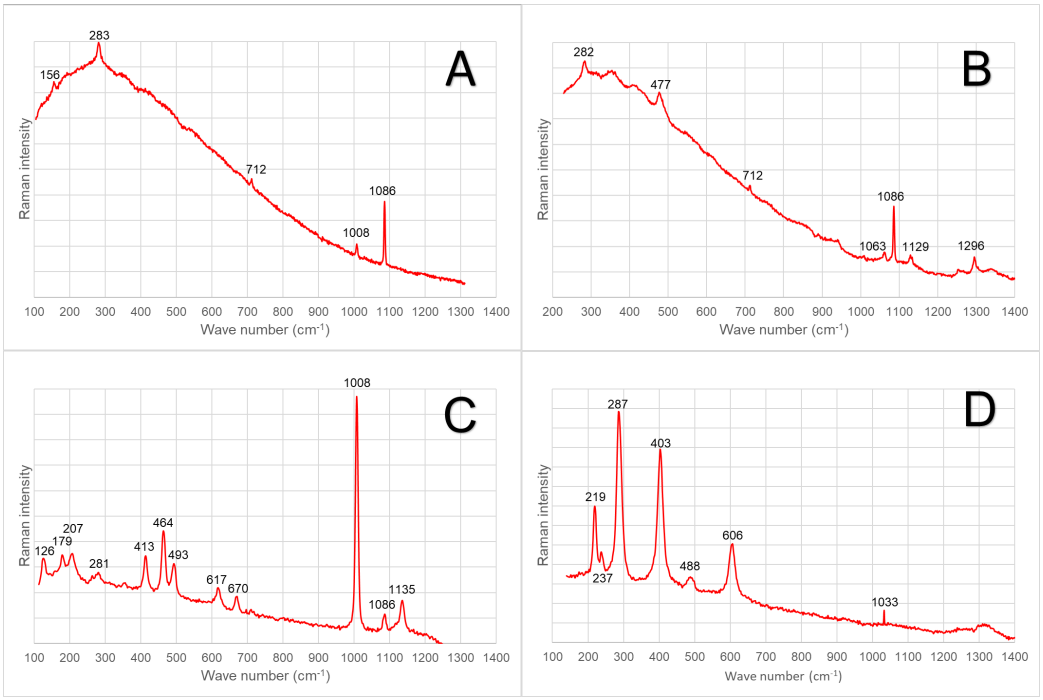

Figure 3: Raman spectra obtained in laboratory of: A) Sample S1, showing the presence of gypsum and calcite; B) Sample S2, showing the presence of calcite and saturated acids; C) Sample M1, showing the presence of calcite, quartz and gypsum; and D) Sample S4 showing the presence of haematite.

was the absence of sodium sulfate and nitrates, in both, in-situ and laboratory analysis. The main bands of thernardite ($NaSO_4$) and mirabilite ($NaSO_4 \cdot 10H_2O$) are around 990 cm^{-1} and these salts can be responsible for the generation of gypsum from calcite or portlandite in limestones and mortars [7, 8]. This is a common concern in the field of durability of building material in zones susceptible to marine aerosol, but was excluded due the overall distribution of the gypsum phase without sodium sulphate peaks. On the other hand, nitrates are often present in underground water and can cause precipitations similar to the ones found at the location through the replacement of the carbonaceous phase and further hydration [9], so it was also useful to eliminate this possibility with the tests.

3.2. X-ray fluorescence

Due to differences in signal intensity, acquisition time and environmental parameters, the counts that can be registered for each detected element spans orders of magnitudes between instruments and settings. In order to provide clear and comparable results, it was decided to normalize the counts registered for each element with each instrument and set-up. Considering that Ca is the major element in the analyzed stones, this element was used as normalizer, dividing in this sense the counts of each element by the counts of Ca registered in the same measuring area (X/Ca). The authors select calcium as a normalisation element because of its presence in all samples. This was expected for limestones and mortar samples, and confirmed by the identification of calcite in each specimen through Raman spectroscopy both in-situ and in laboratory. These results are shown in Figures 4 and 5. The legend is organized regarding device (IS = in-situ; LM = laboratory, mechanical collimator; LP = laboratory, polycapillar collimator), filter (NF = no filter; AF = aluminium 600 μm filter), and method of elemental identification (M = manual; A = using the described algorithm; B = using Bruker software). The data numbers corresponding to the column bars in Figures 4 and 5 are provided as Supplementary Material.

Samples S1 and S2 show strong peaks for chlorine and strontium, both commonly found in locations exposed to marine aerosol [9]. Samples S3 and S4 show a strong presence of iron and strontium. While iron is likely to simply be part of the rocks composition, the high concentration of strontium can be misleading. For those two samples it appears higher than chlorine only in filtered signals, because the aluminium wall weakens the detection of both chlorine and calcium, causing a much higher peak of strontium in proportion. Taking this into account, the presence of both added to the bromine peaks still points strongly to marine aerosol as source. As expected, samples M1 to M4 had strong chlorine, bromine and strontium peaks as well. In addition the usual presence of silicon and iron for mortars is observed. Sample M5 follows the same trend, however, chlorine was detected in much smaller amounts and zinc in much higher quantity. This can be explained by the corrosion of zinc reinforcement, absorbing chlorine to form simonkolleite and bringing zinc closer to the surface [40, 41]. Although no evidence is presented here for this hypothesis, a second experimental campaign (object of a future publication) included more locations of Villa Belza and found clear evidence of the precipitation of simonkolleite in different locations through the use of X-ray diffraction and Raman spectroscopy.

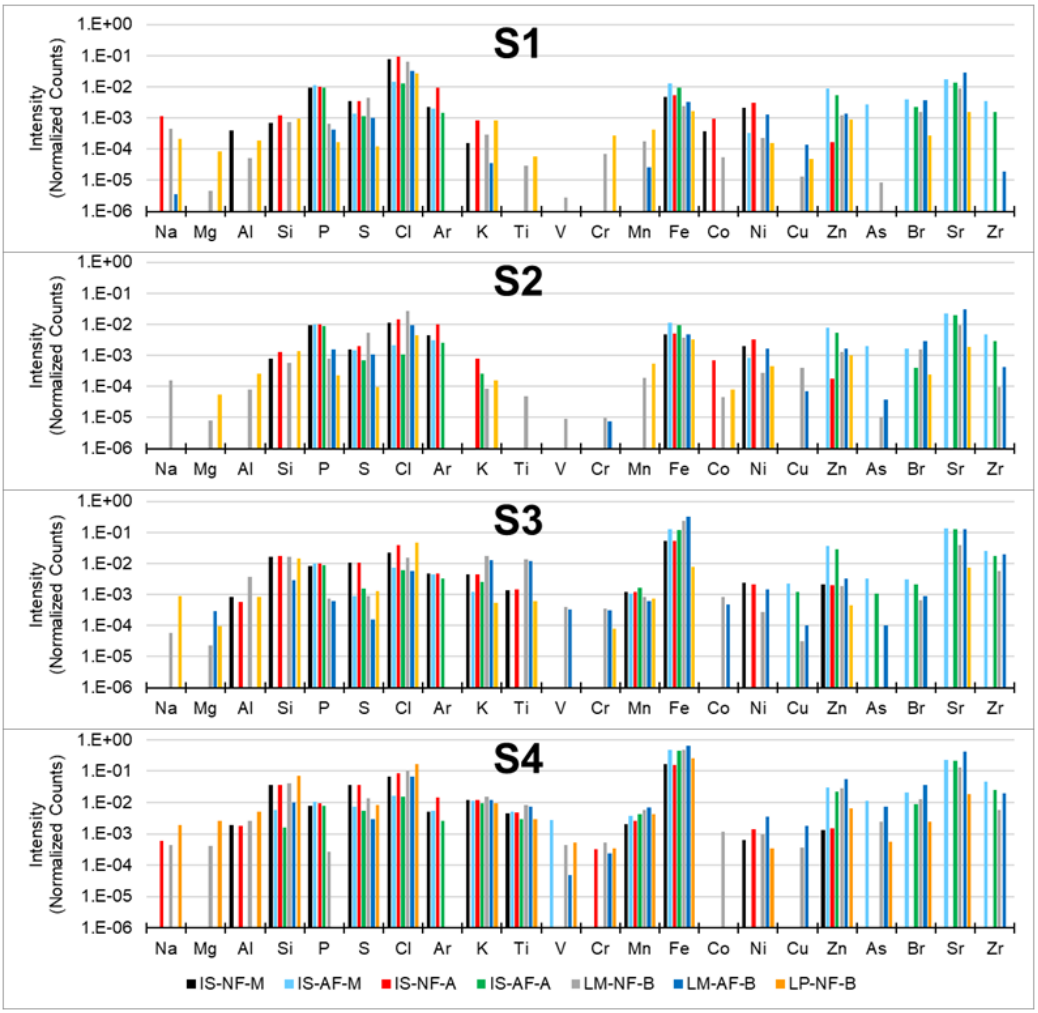

Devices: IS = in-situ; LM = laboratory, mechanical collimator; LP = laboratory, polycapillar collimator.

Filter: NF = no filter; AF = aluminium 600 μm filter.

Method of elemental identification: M = manual; A = using the described algorithm; B = using Bruker software.

Figure 4: X-ray fluorescence results for stone samples.

3.3. In-situ versus laboratory analysis

The selected materials proved challenging to perform molecular analysis, the spectra were saturated more often than not and the surfaces were very rough, which contributed to the disparity between field and lab work. Ultimately, what allowed the detection of more phases in laboratory were the

advantages associated with micro-spectroscopy against the regular type. The greater amount of laser power alternatives in addition to the aid of a light microscope and servo controlled stage allowed for much higher precision in choosing a scanning area, and possibility of tracing the exact spot back in case of change of parameters.

Nevertheless, the Raman analysis performed there did not differ much from what was obtained in-situ. Although some spectra allowed to spot minor inclusions, the overall results still pointed to a predominance of calcite. The identification of the acids and haematite is not a signal of damaging agents in the building materials, but rather small, inert inclusions. Additionally, the absence of sodium sulphate excludes the possibility of damage by the replacement of carbonate phases by sulphates. Thus, the in-situ analysis proved as useful as laboratory testing for the specific goal of this campaign.

Concerning the XRF elemental analysis, the main difference between the spectra collected at the location and the ones extracted afterwards was related to signal intensity. Looking at Figures 4 and 5 it is noticeable that only elements with a X/Ca ratio above 10^{-4} can be identified, while at laboratory the threshold is above 10^{-6}. This discrepancy is a reflection of the vacuum environment and longer exposure time possible with the desktop instrument that provided an absolute amount of counts one to two orders of magnitude superior to the obtained in-situ results. Thus, the overall limit of detection is similar, but the difference in signal quality acts as a hindrance for light and trace elements.

The identification of such trace elements (e. g. vanadium, chromium) are usually of no interest for the forensic analysis of building materials, but information on light elements (e. g. sodium, magnesium, aluminium) can be very valuable. In this particular case, the presence of sodium in the same areas as chlorine support the assumption of sodium chloride from marine aerosol as main agent of degradation. Regardless, damage in building materials caused by ingression of chemicals is normally well distributed through the material and only high concentrations activate considerable deterioration. For elements following this frame of reference (e. g. chlorine, bromine, strontium), the in-situ analysis demonstrated no problems of detection.

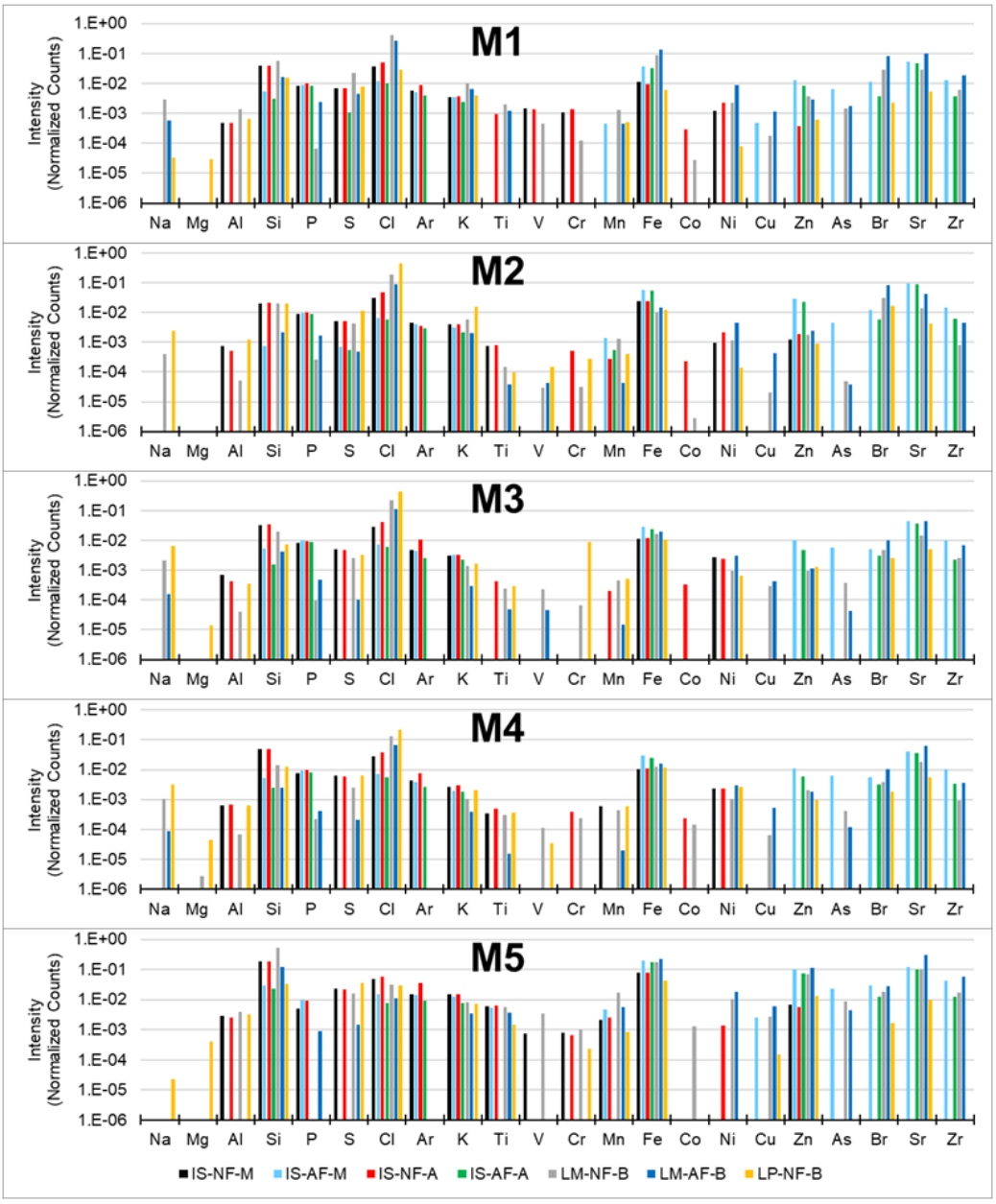

Devices: IS = in-situ; LM = laboratory, mechanical collimator; LP = laboratory, polycapillar collimator.

Filter: NF = no filter; AF = aluminium 600 µm filter.

Method of elemental identification: M = manual; A = using the described algorithm; B = using Bruker software.

Figure 5: X-ray fluorescence results for mortar samples.

3.4. Automatic identification of peaks in XRF spectra

The automatic identification of elements was considered successful given the excellent correlation between the data obtained with EzData^{TM}and with the MATLAB® script. Compared to the elements detected by laboratory analysis, the automatic identification is better for the unfiltered signals, matching more elements than with the manual selection (see Figures 4 and 5). Samples S2 to M3 can be used as examples, where the algorithm correctly identified three additional elements in comparison to the manual procedure (see Figures 4 and 5). It can be seen that the elements missed by the operator are present in very small concentrations, always inferior to 0.001 (as Ca ratio).

The opposite is observed for filtered signals, more elements are successfully identified manually. This can be explained by the poor quality of the signal for in-situ filtered samples. The absolute intensity of the peaks ranges from one to two orders of magnitude smaller than unfiltered spectra. The combination of the high degree of noise with the need for a more complex baseline correction hinders the elemental detection. Sample M5 can serve as an example, the signal for this sample was less intense than for all other samples and consequently, the automatic selection had the worst performance of all samples, finding the same amount of elements in the unfiltered signal and less in the filtered one. For human selection, the baseline correction is not necessary and the noise is not as detrimental, since user experience already adds a bias to always look for peaks at the same energy intervals. Although the data processing can always be improved and new filters are constantly in development, a good signal is still key for accurate automatic detection. In the case presented herein, an increase of acquisition time per spectra would most likely diminish or even eliminate the problem.

Finally, the possibility of an automatic identification of elements brings all the usual advantages of automation, it increases repeatability, decreases the work time from several hours to few seconds and removes human bias. Although the code developed here has limitations, an operator aided version could provide the improvements without sacrificing accuracy.

4. Conclusion

In this paper, an experimental campaign was executed on an 130 years old structure to determine the reason of façade deterioration that motivated a renovation. Considering its exposition to the sea and the presence of visible

salt precipitation, the damage to the façade was found to likely arise from the crystallization pressure developed by sub-florescences. The experiments aimed at determining which were the crystals in action, or at identifying another underlying cause.

A comparison was drawn between in-situ Raman and X-ray fluorescence spectrometry and its laboratory counter parts. After the analysis of several materials at nine distinct locations of the façade in question, it was concluded that the most reasonable cause of deterioration would be the crystallization of sodium chloride. This is corroborated by the absence of sodium sulphate peaks in the molecular analysis and the very high amounts of chlorine detected by XRF. Further, the presence of bromine and strontium points to the sea as a source for the chloride and wind as main means of transport.

Such conclusion could be reached by both in-situ and laboratory results, which highlight all the advantages of in-situ testing stated in the introduction. Although the experiments performed in laboratory provided less noisy signals and overall more information, they did not provided better information. The theory regarding the damage was formulated with data available in both modes of testing and the additional information acquired in laboratory was not essential to deduce the reasons for the façade deterioration. Hence, the authors strongly support the use of hand-held instruments for this application.

Acknowledgments

The authors gratefully acknowledge the financial support from the *Communauté d'agglomération Pau Béarn Pyrénées* and from the *ED211* doctoral school. The authors are also thankful to the TMH restoration company who granted the access to the Villa Belza during its restoration. D. Grégoire is fellow of the *Institut Universitaire de France*.

Figures with Essential Color Discrimination

Certain figures in this article, particularly Figs. 4 and 5 are difficult to interpret in black and white. The full color images can be found in the on-line version.

References

[1] Kronlund, D., Linden, M., Smatt, J.H. A polydimethylsiloxane coating to minimize weathering effects on granite. Construction and Building Materials (2016), Vol. 124, pp. 1051-1058. https://doi.org/10.1016/j.conbuildmat.2016.08.146.

[2] Liu, Z., Li, X., Deng, D., Schutter, G., Hou, L. The role of Ca(OH)2 in sulfate salt weathering of ordinary concrete. Construction and Building Materials (2016), Vol. 123, pp. 127-134. https://doi.org/10.1016/j.conbuildmat.2016.07.006.

[3] Cardell, C., Delalieux, F., Roumpopoulos, K., Moropoulou, A., Auger, F., Van Grieken, R. Salt-induced decay in calcareous stone monuments and buildings in a marine environment in SW France. Construction and Building Materials (2003), Vol. 17, Issue 3, pp. 165-179. https://doi.org/10.1016/S0950-0618(02)00104-6.

[4] Heidari, M., Torabi-Kaveh, M., Chastre, C., Ludovico-Marques, M., Mohseni, H., Akefi, H. Determination of weathering degree of the Persepolis stone under laboratory and natural conditions using fuzzy inference system. Construction and Building Materials (2017), Vol. 145, pp. 28-41. https://doi.org/10.1016/j.conbuildmat.2017.03.230.

[5] Steiger, M. Crystal growth in porous materials - I: The crystallization pressure of large crystals. Journal of Crystal Growth (2005), 282(34), 455469. https://doi.org/10.1016/j.jcrysgro.2005.05.007

[6] Flatt, R. J., Caruso, F., Sanchez, A. M. A., & Scherer, G. W. Chemomechanics of salt damage in stone. Nature Communications (2014), 5, 4823. https://doi.org/10.1038/ncomms5823

[7] Chiker, T., Aggoun, S., Houari, H., Siddique, R. Sodium sulfate and alternative combined sulfate/chloride action on ordinary and self-consolidating PLC-based concretes. Construction and Building Materials (2016), vol. 106, pp. 342-348. https://doi.org/10.1016/j.conbuildmat.2015.12.123.

[8] Saba, M., Quiones-Bolaos, E.E., Lopez, A.L.B. A review of the mathematical models used for simulation of calcareous stone deterioration

in historical buildings. Atmospheric Environment (2018), vol. 180, pp. 156-166. https://doi.org/10.1016/j.atmosenv.2018.02.043.

[9] Morillas, H., Maguregui, M., Trebolazabala, J., & Madariaga, J. M. Nature and origin of white efflorescence on bricks, artificial stones, and joint mortars of modern houses evaluated by portable Raman spectroscopy and laboratory analyses. Spectrochimica Acta - Part A: Molecular and Biomolecular Spectroscopy (2015), 136(PB), 11951203. https://doi.org/10.1016/j.saa.2014.10.006

[10] Arnold, J., Duddu, R., Brown, K., Kosson, D.S. Influence of multi-species solute transport on modeling of hydrated Portland cement leaching in strong nitrate solutions. Cement and Concrete Research (2017), Vol. 100, pp. 227-244. https://doi.org/10.1016/j.cemconres.2017.06.002.

[11] Gibeaux, S., Vázquez, P., Kock, T., Cnudde, V., Thomachot-Schneider, C. Weathering assessment under X-ray tomography of building stones exposed to acid atmospheres at current pollution rate. Construction and Building Materials (2018), Vol. 168, pp. 187-198. https://doi.org/10.1016/j.conbuildmat.2018.02.120.

[12] Tang, Y., Zuo, X., Yin, G., Davoudi, H., Li, X. Influence of calcium leaching on chloride diffusivity in cement-based materials. Construction and Building Materials (2018), Vol. 174, pp. 310-319. https://doi.org/10.1016/j.conbuildmat.2018.04.112.

[13] Freitas, R. P., Coelho, F. A., Felix, V. S., Pereira, M. O., de Souza, M. A. T., & Anjos, M. J. Analysis of 19th century ceramic fragments excavated from Pirenpolis (Gois, Brazil) using FT-IR, Raman, XRF and SEM. Spectrochimica Acta - Part A: Molecular and Biomolecular Spectroscopy (2018), 193, 432439. https://doi.org/10.1016/j.saa.2017.12.047

[14] Koleini, F., Colomban, P., Antonites, A., & Pikirayi, I. Raman and XRF classification of Asian and European glass beads recovered at Mutamba, a southern African Middle Iron Age site. Journal of Archaeological Science: Reports, 13(March, 2017), 333340. https://doi.org/10.1016/j.jasrep.2017.04.004

[15] Franquelo, M. L., Duran, A., Castaing, J., Arquillo, D., & Perez-Rodriguez, J. L. XRF, -XRD and -spectroscopic techniques for revealing the composition and structure of paint layers on polychrome

sculptures after multiple restorations. Talanta (2012), 89, 462469. https://doi.org/10.1016/j.talanta.2011.12.063

[16] Antunes, V., Candeias, A., Miro, J., Carvalho, M. L., Dias, C. B., Manhita, A., Manso, M. Analytical characterization of the palette and painting techniques of Jorge Afonso, the great 16th century Master of Lisbon painting workshop. Spectrochimica Acta - Part A: Molecular and Biomolecular Spectroscopy (2018), 193, 264275. https://doi.org/10.1016/j.saa.2017.12.027

[17] Morillas, H., Garca-Galan, J., Maguregui, M., Marcaida, I., Garca-Florentino, C., Carrero, J. A., & Madariaga, J. M. Assessment of marine and urban-industrial environments influence on built heritage sandstone using X-ray fluorescence spectroscopy and complementary techniques. Spectrochimica Acta - Part B Atomic Spectroscopy (2016), 123, 7688. https://doi.org/10.1016/j.sab.2016.07.015

[18] Prieto-Taboada, N., Ibarrondo, I., Gmez-Laserna, O., Martinez-Arkarazo, I., Olazabal, M. A., & Madariaga, J. M. Buildings as repositories of hazardous pollutants of anthropogenic origin. Journal of Hazardous Materials (2013), 248249(1), 451460. https://doi.org/10.1016/j.jhazmat.2013.01.008

[19] Morillas, H., Maguregui, M., Paris, C., Bellot-Gurlet, L., Colomban, P., & Madariaga, J. M. The role of marine aerosol in the formation of (double) sulfate/nitrate salts in plasters. Microchemical Journal (2015), 123, 148157. https://doi.org/10.1016/j.microc.2015.06.004

[20] Ogburn, D., Sillar, B., & Sierra, J. C. Evaluating effects of chemical weathering and surface contamination on the in situ provenance analysis of building stones in the Cuzco region of Peru with portable XRF. Journal of Archaeological Science (2013), 40(4), 18231837. https://doi.org/10.1016/j.jas.2012.09.023

[21] Garcia-Florentino, C., Maguregui, M., Morillas, H., Marcaida, I., & Madariaga, J. M. A fast in situ non-invasive approach to classify mortars from a construction of high historical value. Microchemical Journal (2017), 133, 104113. https://doi.org/10.1016/j.microc.2017.03.020

[22] Garcia-Florentino, C., Maguregui, M., Margu, E., Torrent, L., Queralt, I., & Madariaga, J. M. Development of Total Reflection X-ray fluorescence spectrometry quantitative methodologies for elemental characterization of building materials and their degradation products. Spectrochimica Acta Part B: Atomic Spectroscopy (2018), 143, 1825. https://doi.org/10.1016/j.sab.2018.02.008

[23] Grantham, M. G. Concrete Repair A Practical Guide. Taylor & Francis (2011), New York, USA.

[24] Bergamo, O., Campione, G., Donadello, S., & Russo, G. In-situ NDT testing procedure as an integral part of failure analysis of historical masonry arch bridges. Engineering Failure Analysis (2015), 57, 3155. https://doi.org/10.1016/j.engfailanal.2015.07.019

[25] Kilic, G. Using advanced NDT for historic buildings: Towards an integrated multidisciplinary health assessment strategy. Journal of Cultural Heritage (2015), 16, 526-535.

[26] La villa Belza. Pays Basque 1900. Available at: http://www.paysbasque1900.com/2014/01/la-villa-belza.html as of 19 of July of 2018.

[27] Maguregui, M., Prieto-Taboada, N., Trebolazabala, J., Goienaga, N., Arrieta, N., Aramendia, J., Gomez-Nubla, L., Sarmiento, A., Olivares, M., Carrero, J.A., Martinez-Arkarazo, I., Castro, K., Arana, G., Olazabal, M.A., Fernandez, L.A., Madariaga, J.M., 2010. CHEMCH 1st International Congress Chemistry for Cultural Heritage, Ravenna, 30th June - 3rd July.

[28] Ian M. Bell, Robin J.H. Clark and Peter J. Gibbs, Raman Spectroscopic Library of Natural and Synthetic Pigments, Christopher Ingold Laboratories, University College London. Available at: http://www.chem.ucl.ac.uk/resources/raman Accessed 08/02/2018.

[29] Downs, R.T., Hall-Wallace, M., A database of crystal structures published in the American mineralogist and the Canadian mineralogist and its use as a resource in the classroom. 18th General Meeting of the International Mineralogical Association, (2002) p. 128.

[30] Mendonça Filho, F. F, Morillas, H., Derluyn, H., Maguregui, M, & Grégoire, D. MATLAB code for XRF spectral analysis, Mendeley Data (2018). [dataset]

[31] J. A. Bearden, X-Ray Wavelengths, Review of Modern Physics, (January 1967) pp. 86-99.

[32] Wang, H. S., Lineweaver, C. H., & Ireland, T. R. The elemental abundances (with uncertainties) of the most Earth-like planet. Icarus (2018), 299, 460474. https://doi.org/10.1016/j.icarus.2017.08.024

[33] Brandon, D. & Kaplan, W. D. Microstructural Characterization of Materials, Second Edition. John Wiley & Sons Ltd (2008), West Sussex, England.

[34] Ning, X., Selesnick, I. W., Duval, L. Chromatogram baseline estimation and denoising using sparsity (BEADS). Chemometrics and Intelligent Laboratory Systems, 139 (2014) 156167. https://doi.org/10.1016/j.chemolab.2014.09.014

[35] Huang, N., Short, M., Zhao, J., Wang, H., Lui, H., Korbelik, M., & Zeng, H. Full range characterization of the Raman spectra of organs in a murine model. Optics Express (2011), 19(23), 22892. https://doi.org/10.1364/OE.19.022892

[36] Banfill, P.F.G., Szadurski, E.M., Forster, A.M. Deterioration of natural hydraulic lime mortars, II: Effects of chemically accelerated leaching on physical and mechanical properties of carbonated materials. Construction and Building Materials (2016), Vol. 111, pp. 182-190. https://doi.org/10.1016/j.conbuildmat.2016.02.055.

[37] Yoon, I.-S. Deterioration of concrete due to combined reaction of carbonation and chloride penetration: Experimental study. Key Engineering Materials (2007), vol. 348, pp. 729 732.

[38] Malheiro, R., Camoes, A., Ferreira, R. M., Meira, G., Amorim, T. & Reis, R. Influncia da carbonatao no transporte de cloretos em argamassas submetidas ao combinada destes dois agentes, in Proceedings of the Congresso Luso-Brasileiro de Materiais de Construo Sustentveis (2014), vol. 1, pp. 479487.

[39] Zhu, X., Zi, G., Cao, Z., & Cheng, X. Combined effect of carbonation and chloride ingress in concrete. Construction and Building Materials (2016), vol. 110, pp. 369 380.

[40] Zhang, Xian; Leygraf, Christofer; Odnevall Wallinder, Inger, Atmospheric corrosion of Galfan coatings on steel in chloride-rich environments. Corrosion Science (2013), vol. 73, pp. 62-71.

[41] Cousy, Simon; Gorodylova, Nataliia; Svoboda, Ladislav; Zelenka, Jiri, Influence of synthesis conditions over simonkolleite/ZnO precipitation. Chemical Papers (2017), vol. 71(12), pp. 2325-2334.